



Roland G. Huber
Structure and Function of RNA

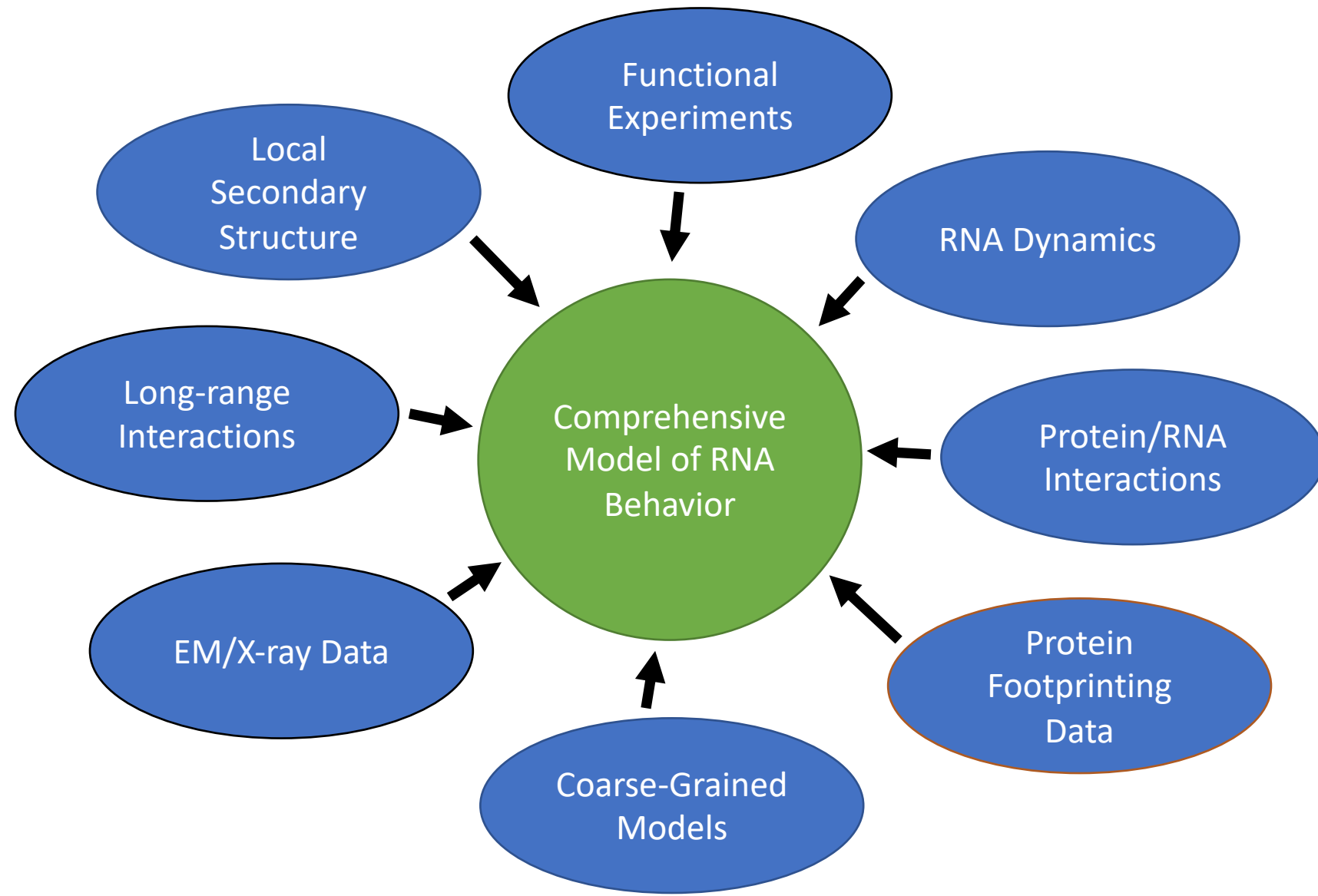
Bioinformatics
Institute

BII

Functional RNA structure as targets for new therapeutics

BII Scientific Conference

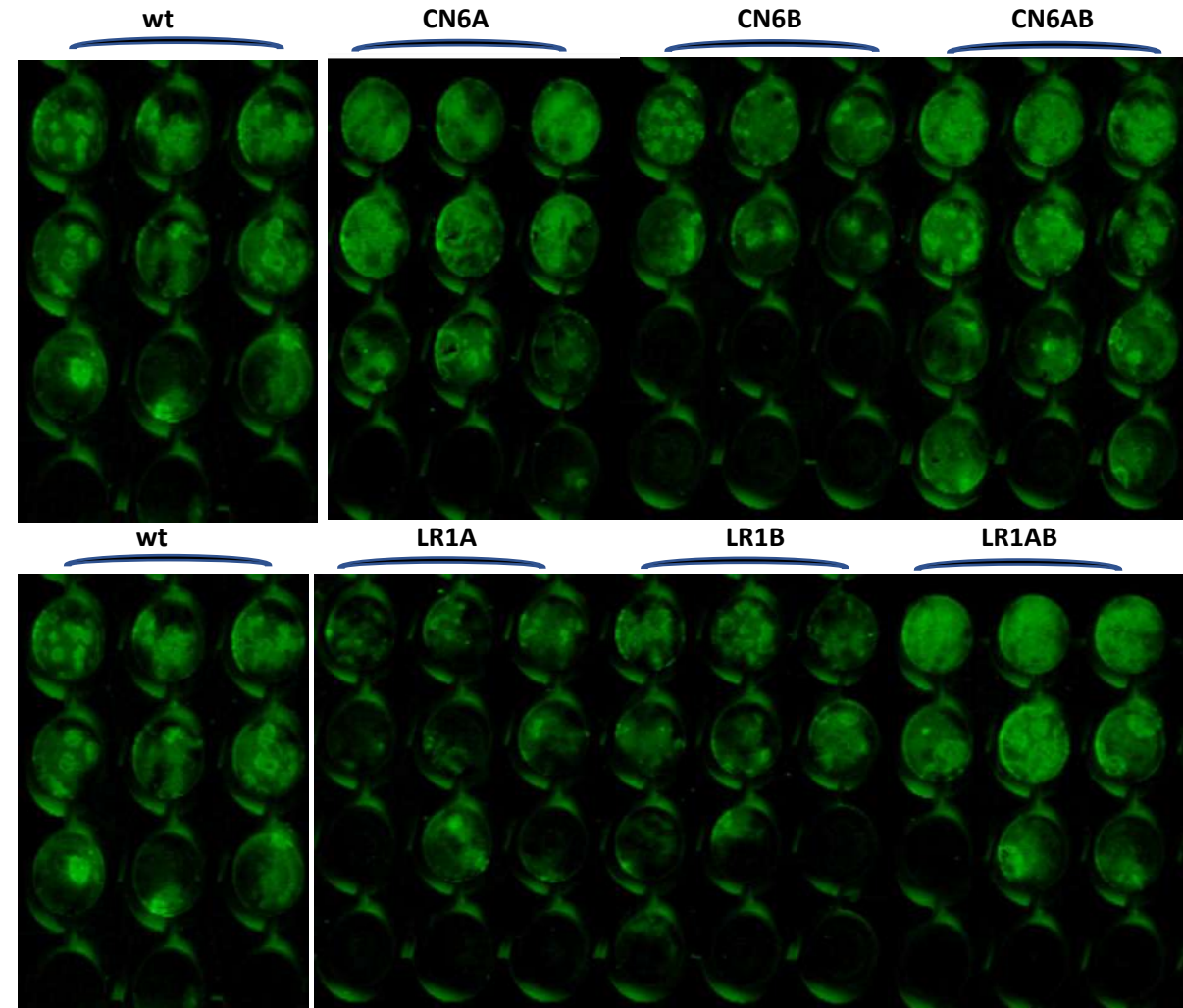
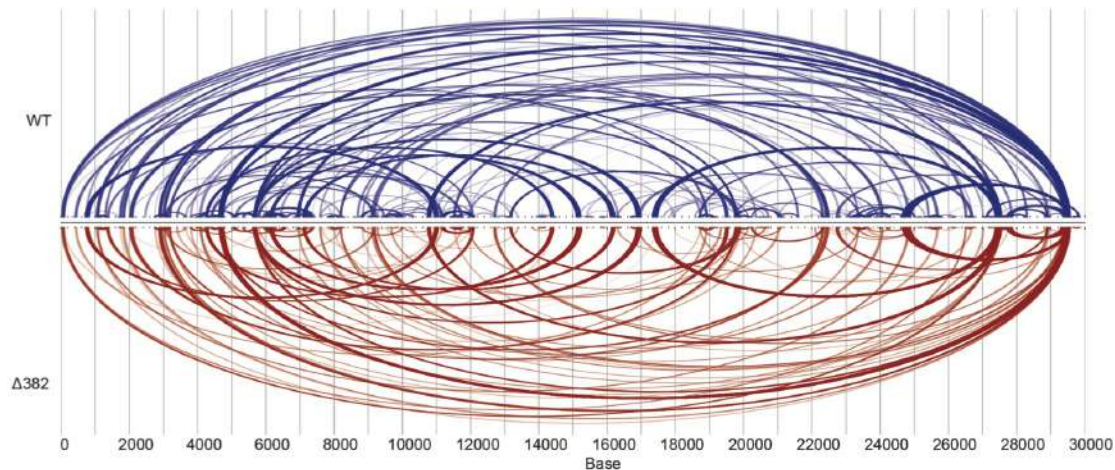
Roland's Lab



SARS-CoV-2 Genome Structure

We identified crucial structural elements in the genome of SARS-CoV-2 through chemical cross-linking, SHAPE probing and usage of Nanopore sequencing to analyze the individual subgenomic transcripts of the virus.

This allowed us to design mutations within these elements that disrupt these structures and cause significant attenuation of viral fitness. Mutations were designed on both sides of the strand and tested as A/B, and A+B to confirm the effect is related to the predicted structures. Our study offers the potential to design attenuated strains and targeted therapies toward these elements.

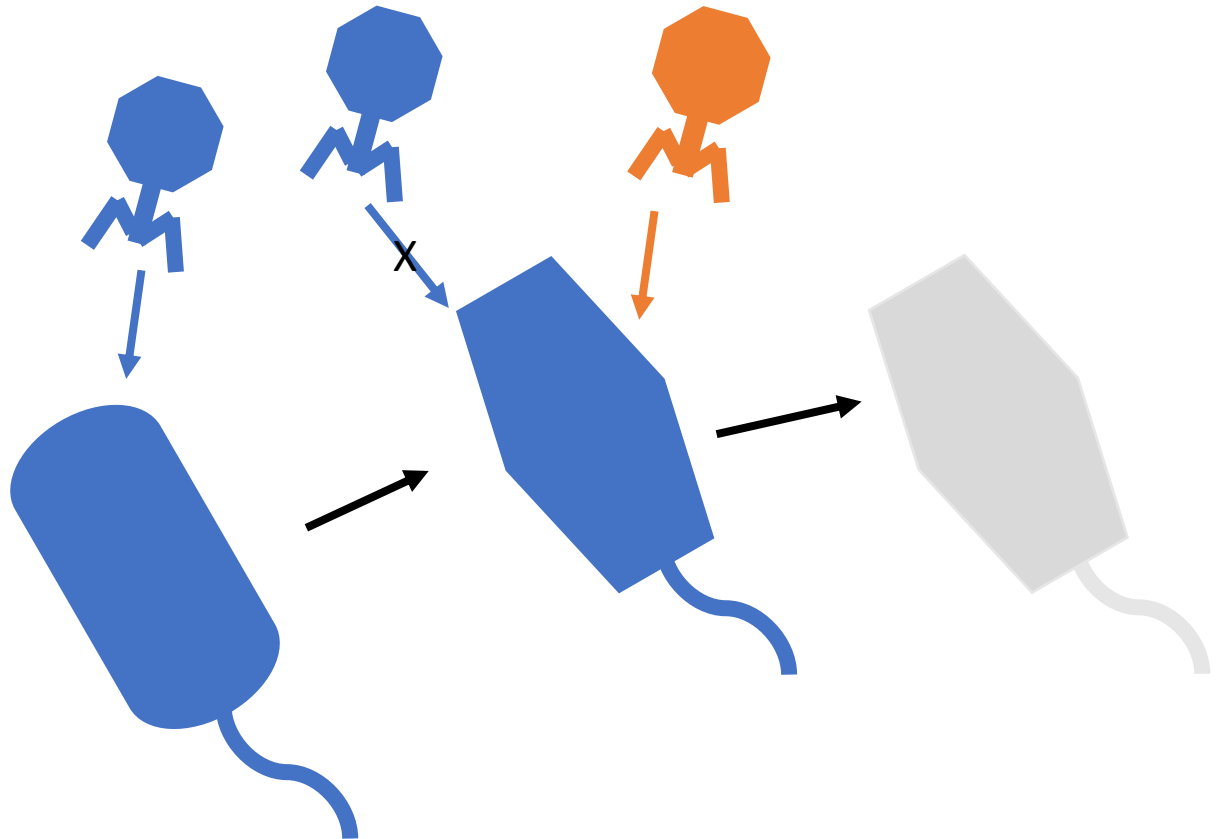


Phage Therapy for antibiotic-resistant bacteria

Antimicrobial resistance is a serious concern. Antibiotic-resistant bacterial infections are a rising cause of mortality around the world and new approaches are necessary to address this health concern. This project aims to establish phage therapy as a viable strategy in the treatment of such infections.

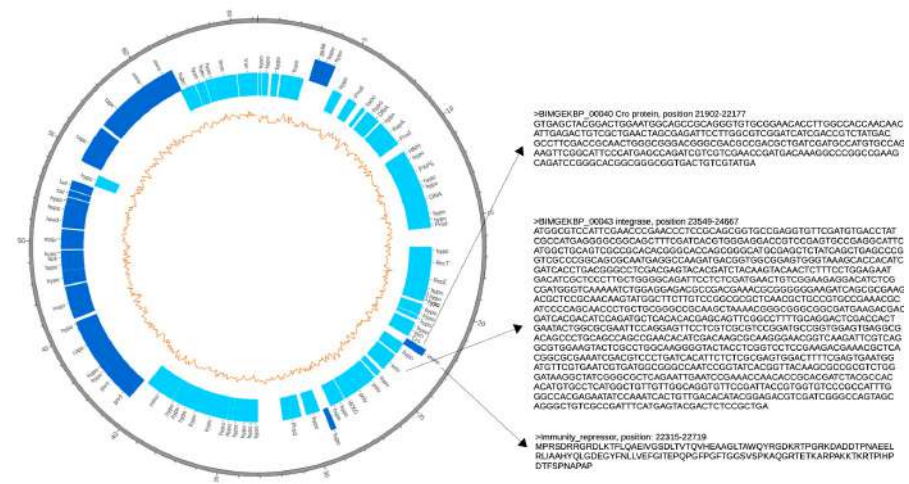
Phage therapy faces challenges in that bacteria are quickly developing resistance. The emergence of resistance is often associated with significant changes in bacterial morphology up to and including the complete loss of an outer membrane which makes them immune from further phage infections.

Combination phage therapy we are developing uses combinations of phages where a cocktail of phages is administered where emergence of resistance to one cocktail component makes the bacteria susceptible to infection by other components.

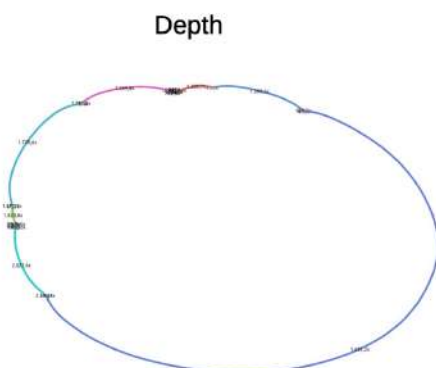


Phage Therapy for antibiotic-resistant bacteria

We are working on genome assembly and annotation and the design of recombinant phages to establish lytic behaviour. Phage infection can lead to either the integration of the phage genome into the host (lysogenic behaviour) or the lethal infection of the bacterium (lytic behaviour). Lytic phages can be obtained by excising or inactivating certain genetic elements responsible for integration.

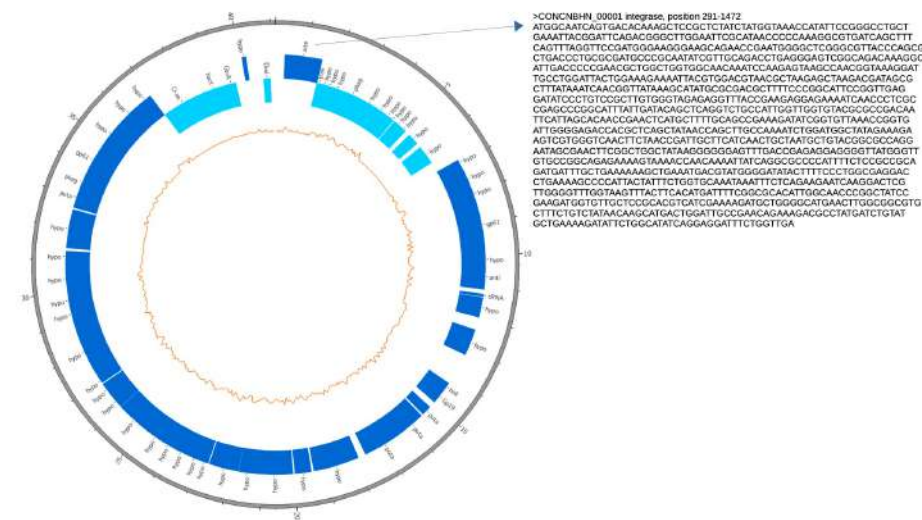


Assembly and scaffolds



Graph size		Node sizes	
Node count:	2,345	N50:	372 bp
Edge count:	42	Shortest node:	78 bp
Edge overlaps:	77 bp	Lower quartile node:	250 bp
Total length:	938,771 bp	Median node:	275 bp
Total length (no overlaps):	936,307 bp	Upper quartile node:	377 bp
		Longest node:	40,479 bp
Graph connectivity		Depth	
Dead ends:	4,626	Median depth:	1,21x
Percentage dead ends:	98,64%	Estimated sequence length:	83,138,799 bp
Connected components:	2,317		
Largest component:	68,936 bp (7,34%)		
Total length orphaned nodes:	869,469 bp (92,62%)		

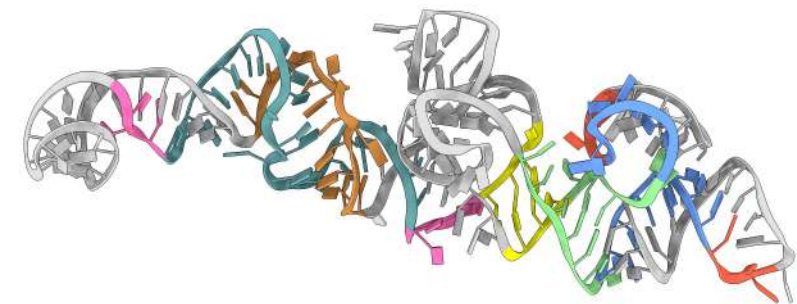
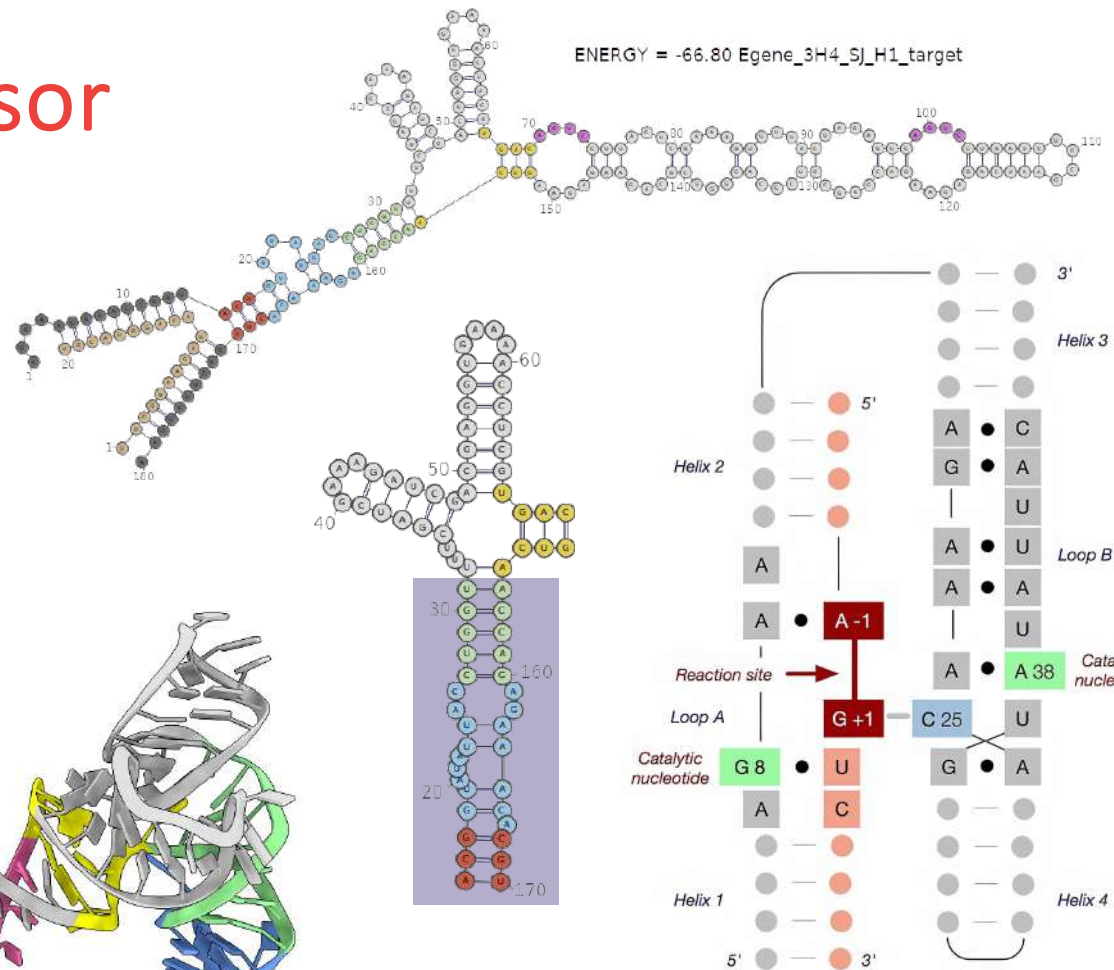
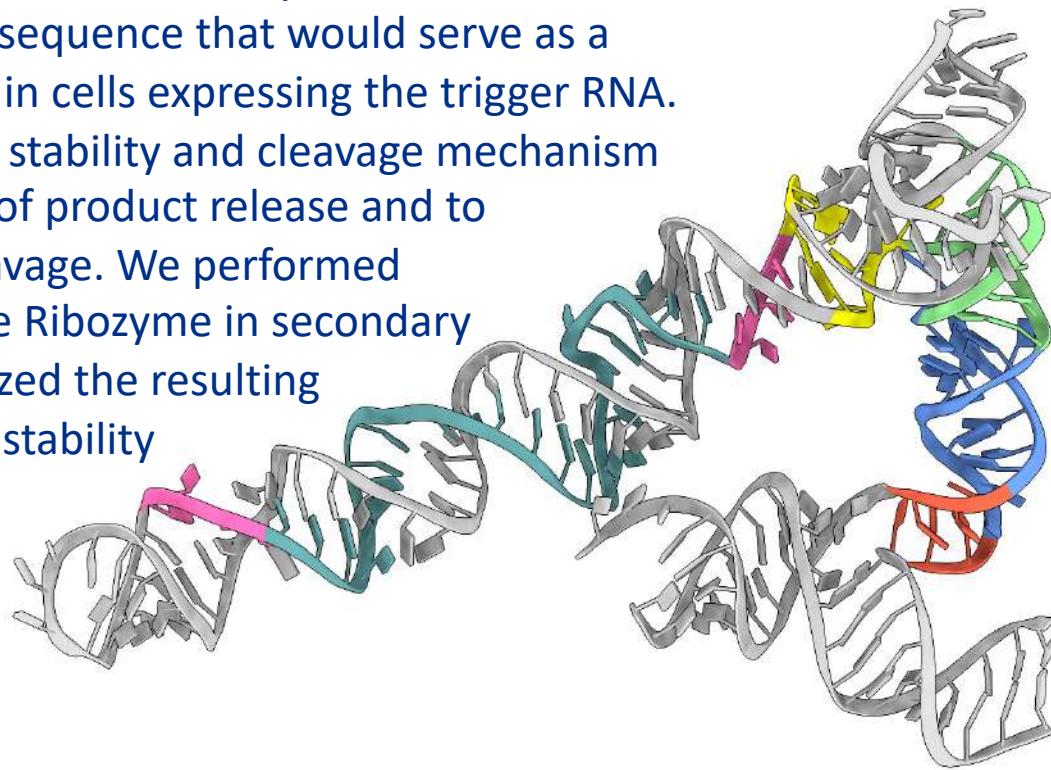
	Genome size	Max scaffold	Min scaffold	Median Depth	GC content
Jabs (7 scaffolds)	66,251	40,479	833	1,47x	0.64





Ribozyme Biosensor

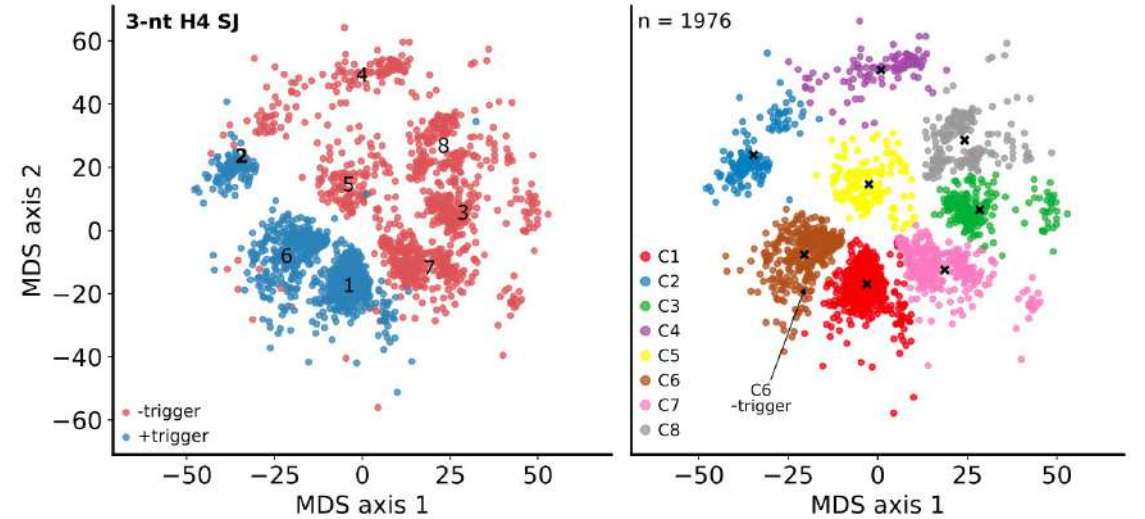
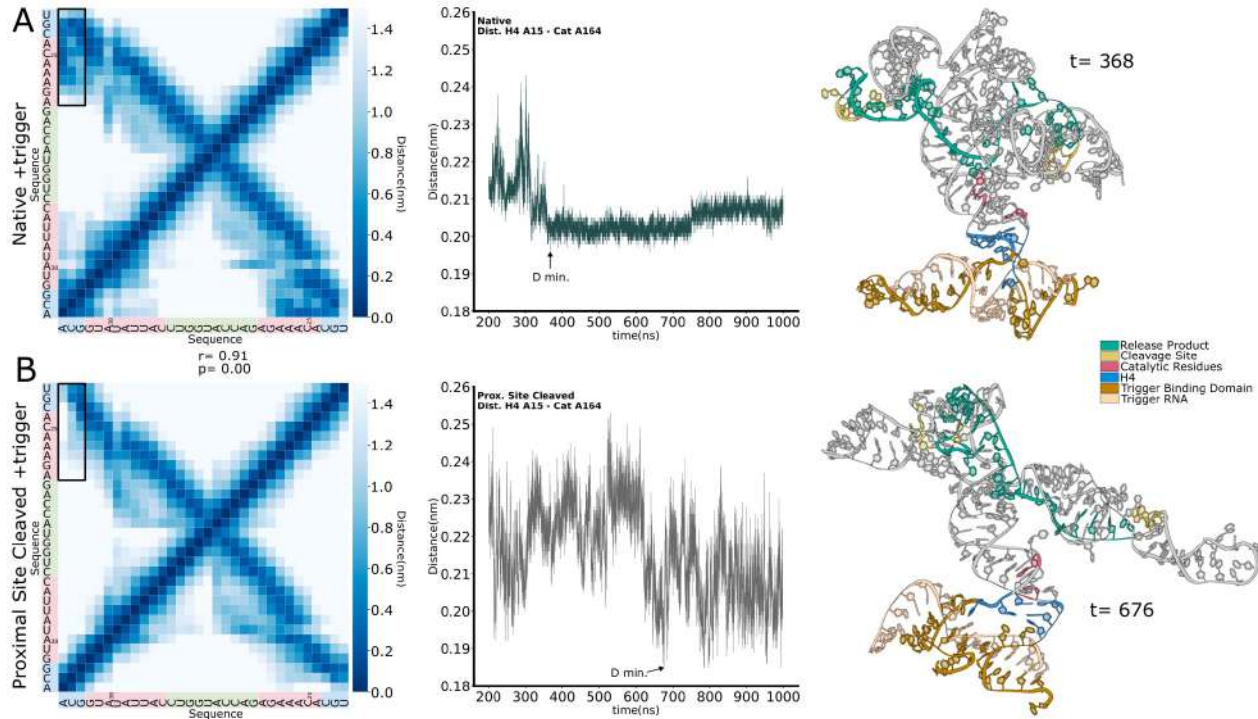
The lab of Sherry Aw designs RNA constructs for diagnostic and therapeutic purposes. We contribute to the design of an autocatalytic ribozyme triggered by specific small RNAs. This strategy offers the opportunity to create biosensors via the release of fluorescent probe RNAs in the presence of disease-specific small RNAs. Alternatively, the constructs can release any specific small sequence that would serve as a targeted therapeutic only in cells expressing the trigger RNA. Our team investigates the stability and cleavage mechanism to improve the efficiency of product release and to minimize background cleavage. We performed extensive modelling of the Ribozyme in secondary structure space and analyzed the resulting Ensembles with regard to stability and energetics. We also proceeded to model the cleavage dynamics using MD simulations.





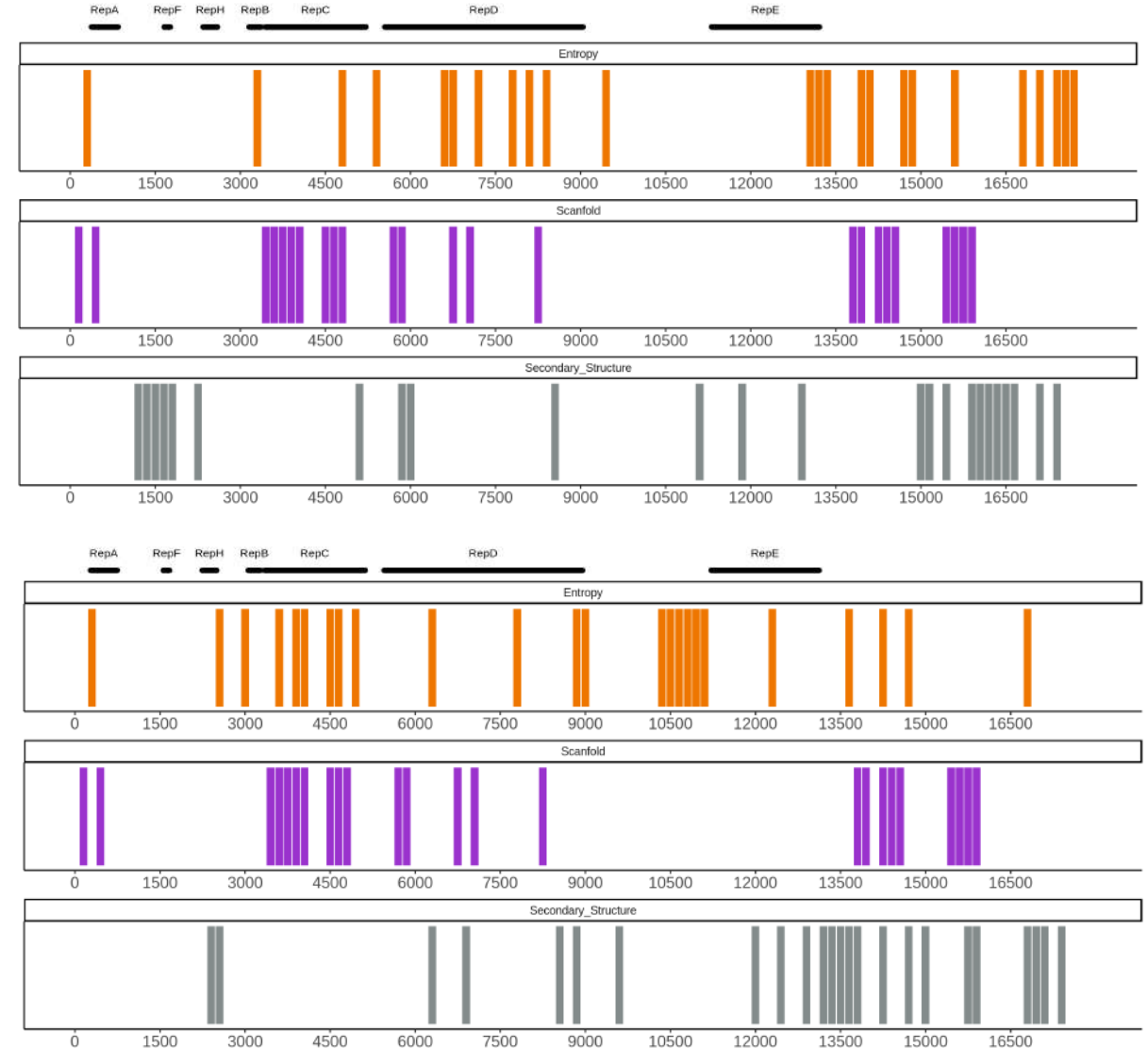
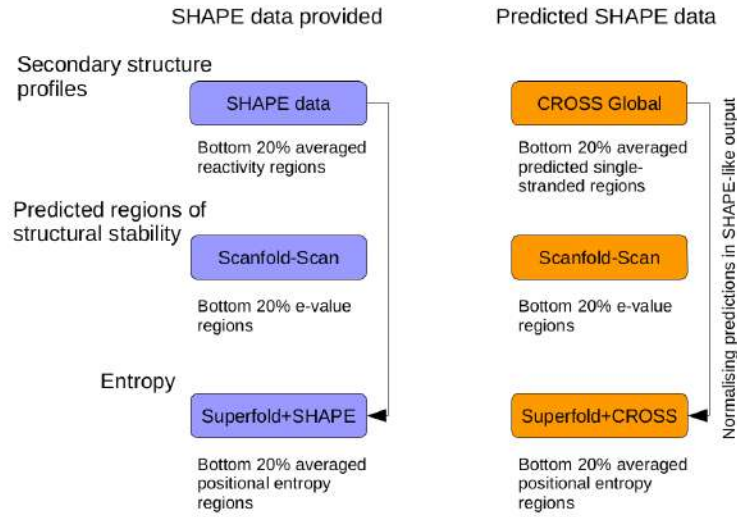
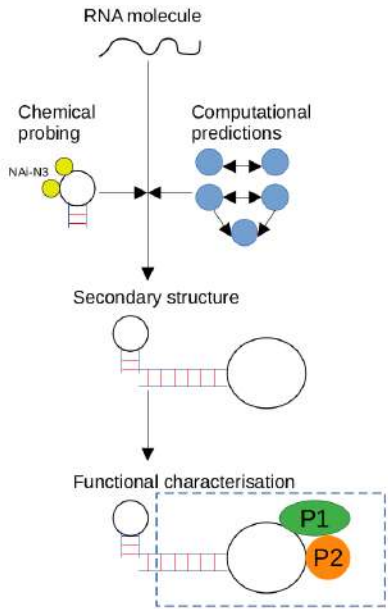
Ribozyme Biosensor

We have conducted simulations to understand the observed one-sided cleavage of the release product. Initial cleavage at the proximal site induces a level of destabilization on the biosensor, particularly the trigger-stabilized H4 region and thus reduces reactivity for distal site cleavage.



If the H4 helix is properly designed and at the ideal level of stability, trigger binding is the deciding factor that shifts the structural ensemble to a catalytically active one. If the stability of H4 is too high, autocatalysis in the absence of trigger will be significant, leading to high levels of noise. If the stability in the presence of trigger is insufficient, catalytic activity will be limited, impacting sensitivity. Careful study of ensembles allowed us to identify the energetic sweet spot of stability and structurally understand biosensor behaviour.

RNAnavigator



We constructed a computational pipeline to streamline the analysis of structure probing data and secondary structure modelling in the analysis of RNA structure. In the absence of experimental reactivity data, we include CROSS data that uses machine learning to impute reactivity from sequence. We show that our pipeline is able to identify known functional RNA segments in viral genomes, mRNAs and lncRNAs.



Evolution of RNA structure

Conceived as a follow-up to the neurogenesis project, we are currently investigating the evolutionary conservation of mRNA and ncRNA structure in mammals. We were able to identify a high number of orthologous genes and our collaborators performed full-transcriptome structure probing. We are currently comparing structures of all covered orthologous transcripts between species to identify conserved structural elements despite sequence changes.

Species	Total Genes	>50%	>80%	Orthogroups of 9 species	Orthogroups (9 species) >50%	Orthogroups (9 species) >80%
Human	23'325	12'795 (55%)	5'333 (23%)	6'508 (28%)	4'093 (17%)	2'149 (9%)
Green Monkey	1'972	1'082 (55%)	481 (24%)	1'401 (71%)	768 (39%)	359 (18%)
Mouse	7'891	4'840 (61%)	2'285 (29%)	2'583 (33%)	1'735 (22%)	990 (13%)
Dog	6'265	4'475 (71%)	2'563 (41%)	3'978 (63%)	2'979 (48%)	1'824 (29%)
Pig	3'841	2'103 (55%)	1'011 (26%)	2'473 (64%)	1'394 (36%)	694 (18%)
Rat Kangaroo	832	149 (18%)	21 (2%)	596 (71%)	99 (12%)	12 (1%)

